Effects of wall roughness on flow in nanochannels

Filippos D. Sofos, Theodoros E. Karakasidis,[*] and Antonios Liakopoulos

Hydromechanics and Environmental Engineering Laboratory, School of Engineering, University of Thessaly,
38834 Pedion Areos, Volos, Greece

Nonequilibrium molecular dynamics simulation is applied to investigate the effect of periodic wall roughness on the flow of liquid argon through krypton nanochannels. The effect of the length of a rectangular protrusion on the flow is investigated and compared to the case of nanochannels with flat walls. The results show a clear trapping of fluid atoms inside the rectangular cavities that are formed between successive protrusions. The size of the cavities affects the potential energy map and, consequently, fluid atom localization. This localization results in a reduction of velocity values inside the cavities, as well as a reduction of the slip length near the rough wall.

I. INTRODUCTION

The assumption that a flowing fluid is immobilized near solid walls (the "no-slip condition" assumed at the wall in ordinary fluid dynamics) has to be revised when dealing with flows in nanochannels. The width of the nanochannel, the structure of the solid boundary, and the type of fluid-solid interaction near a solid wall are expected to play a significant role in the flow properties at the nanoscale. It has been shown in great detail [1–8] that the channel width is of particular importance. In small channel widths, the fluid is inhomogeneous near the solid boundary and the Navier-Stokes hydrodynamic prediction for the velocity profile and the no-slip condition break down.

Another critical aspect that affects fluid behavior at the boundary is the wall-fluid interaction, which characterizes a wetting (small wall-fluid interaction) or a nonwetting (large wall-fluid interaction) surface. In [9,10] it was found that, as the wall-fluid interaction increases, larger peak maxima and more oscillations are generated in the density profile close to the solid walls. In [11], useful results on density, velocity, and temperature profiles and the slip length in a channel of width $h=16\sigma$ with different wettability conditions on the solid interface are reported.

The effect of wall structure is also of particular importance in nanoflows, since wall roughness becomes significant compared to the channel dimensions. There are various classifications of wall roughness in the literature. Nevertheless, at the atomic scale, the definition of a smooth wall is somewhat imprecise since the walls are formed by individual particles with finite roughness [12]. Priezjev in [13] also defines thermal wall roughness to depend on the kind of forces of the wall atoms. He represented it with the spring constant and found that thermally smooth walls are achieved by increasing the wall atom spring constant. Galea and Attard [14] study the effect of wall roughness by varying the size and spacing between solid atoms and keeping the interaction with the fluid atoms constant. They examine the effect of wall roughness on slip length and find that the slip length

presents a nonmonotonic behavior as the wall varies from smooth to rough.

Work has been reported on rough walls with various geometrical patterns. In a triangular-shaped wall [15] it was found that fluid velocity values decrease near the walls as the roughness amplitude increases. Ziarani and Mohamad [16] consider a channel with random roughness patterns at the walls and report on velocity fluctuations as the roughness amplitude increases. Jabbarzadeh *et al.* [17] studied the flow of liquid hexadecane in sinusoidal-wall channels and concluded that slip at the wall increases as the roughness period increases, for the specific length of hexadecane molecules. Kim and Darve [18] studied electro-osmotic flow of water molecules through channels with rectangular roughness and present density profiles that show "layering" near the walls. The layering follows the shape of the wall surface. Velocity values are smaller inside roughness steps and the diffusion coefficient tends to be smaller near the rough wall. Priezjev [13] studied random and periodic rough walls by varying the roughness amplitude of the wall surface and presented results on the variation of slip length as a function of the local shear rate.

Apart from molecular dynamics, surface slippage has been examined with mesoscopic lattice Boltzmann approaches in [19,20], where it was suggested that it is possible to design smart surfaces with controlled slippage. Slip length was also estimated by hydrodynamic calculations for rough boundaries in [21] and for rough boundaries with controlled hydrophobicity (superhydrophobic surfaces) in [22]. Experimental results for flows past superhydrophobic surfaces are reported in [23,24], where it is concluded that fluid atoms do not enter roughness cavities due to the existence of an air/water interface.

Further insight into the effects of wall roughness on fluid flows in conduits is warranted. For example, fluid atoms could possibly be trapped inside the cavities of a rough wall or, on the contrary, they could be forced away because of the increased interaction with wall atoms. The present work investigates fluid atom behavior in channel layers adjacent to a rough wall formed by periodically spaced rectangular protrusions. Potential energy plots are presented in order to reveal probable positions of fluid atoms close to and inside the rectangular grooves. We also present detailed density and veloc-

*thkarak@uth.gr
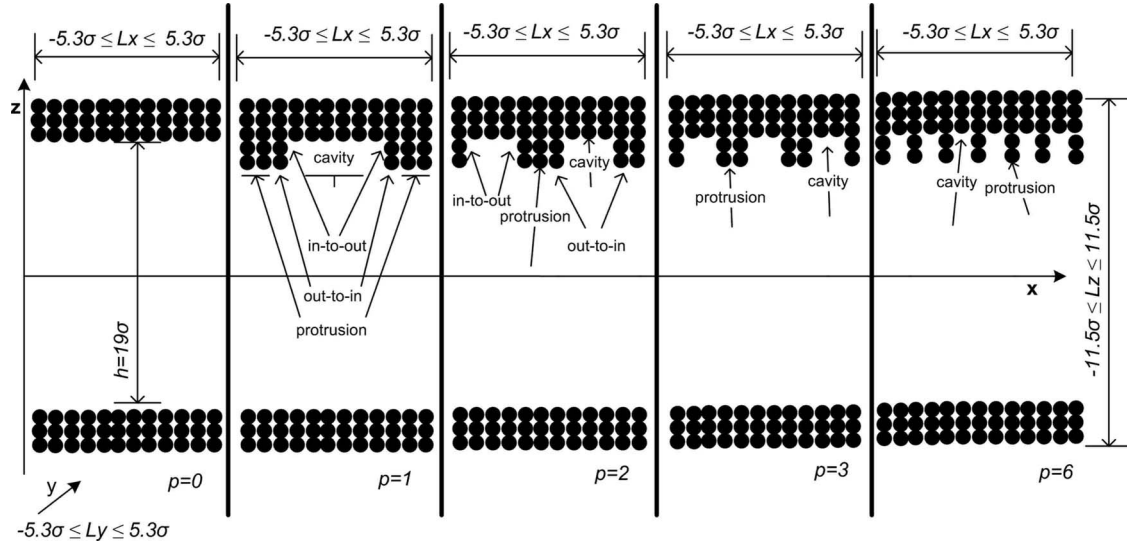
FIG. 1. Schematic of channels modeled.

ity profiles calculated over a dense computational grid inside the nanochannel. Moreover, we investigate fluid atom trapping inside roughness cavities by analyzing their trajectories. Finally, slip length at the boundary is estimated as the roughness period varies.

The present paper is set up as follows. In Sec. II simulation details are presented. Results are presented and discussed in Sec. III, and Sec. IV contains concluding remarks.

II. SIMULATION DETAILS

A. Molecular system model

Nonequilibrium molecular dynamics simulations were performed to simulate the flow of liquid argon in a channel with krypton walls. The lower wall of the channel is smooth. The rough upper wall is constructed by "adding" extra wall atoms to form periodically spaced rectangular protrusions (see Fig. 1). We considered five different cases for the periodic roughness of the upper wall ($p=0$, 1, 2, 3, and 6, as shown schematically in Fig. 1), where p represents the number of rectangular grooves in the computational domain, i.e., $p=0$ is the smooth channel, $p=1$ signifies one rectangular groove, $p=2$ two rectangular grooves, $p=3$ three rectangular grooves, and $p=6$ six rectangular grooves. The dimensions of the computational domain in the x, y, and z directions are $L_x \times L_y \times L_z = 10.6 \times 10.6 \times 23$ (in units of σ), while the smooth channel is of width $h=19\sigma$. The roughness amplitude is about 10% of the channel width ($\approx 2\sigma$) and the protrusion
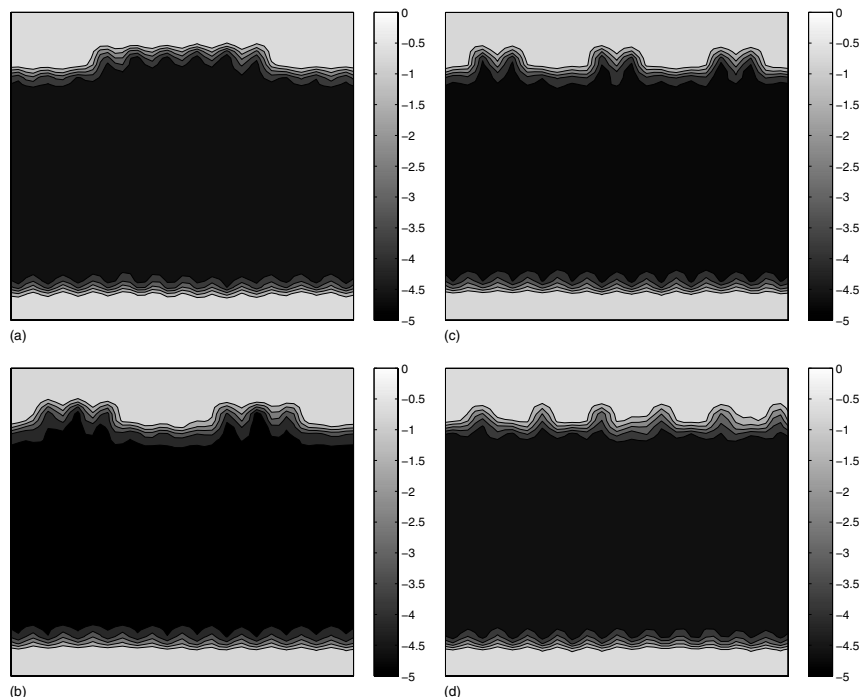
FIG. 2. Potential energy contour plots for $p=$(a) 1, (b) 2, (c) 3, and (d) 6. Light gray regions are the solid walls.
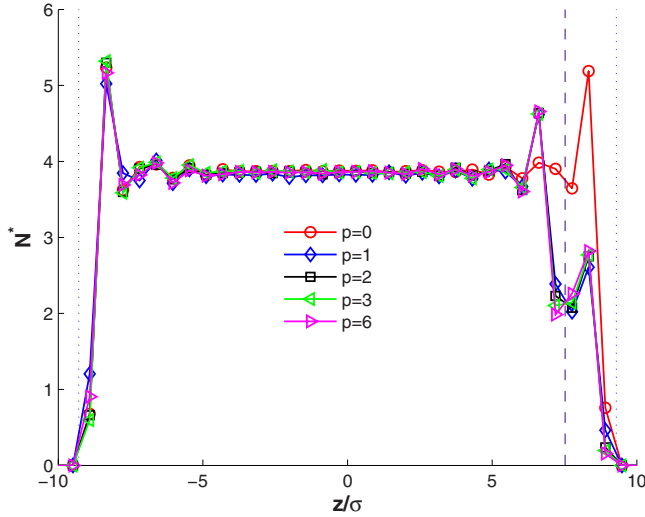
FIG. 3. (Color online) Total average number density profiles. Solid lines are a guide for the eye. Dashed lines denote the protrusion limits and dotted lines the cavities and lower wall limits.

length (and, equivalently, the cavity length) l_g equals $L_x/2p$ (i.e., $l_g=5.3\sigma$, 2.65σ, 1.77σ, and 0.88σ for $p=1$, 2, 3, and 6 respectively). We also performed simulations for a computational domain with dimensions $L_x \times L_y \times L_z = 21.2 \times 10.6 \times 23$ (in units of σ), i.e., we doubled the x dimension so as to investigate the possible existence of size effects, and we obtained the same results for the calculated quantities (within statistical error).

The particle interactions are described by the Lennard-Jones (LJ) 12-6 potential

$$u^{\mathrm{LJ}}(r_{ij}) = 4\varepsilon[(\sigma/r_{ij})^{12} - (\sigma/r_{ij})^{6}], \qquad (1)$$

where the parameters of the Lennard-Jones potential are $\sigma_{\mathrm{Ar\text{-}Ar}}=0.3405$ nm (from now on $\sigma_{\mathrm{Ar\text{-}Ar}}$ will be referred to as σ), $\sigma_{\mathrm{Kr\text{-}Kr}}=0.3633$ nm, $\sigma_{\mathrm{Ar\text{-}Kr}}=0.3519$ nm, $\varepsilon_{\mathrm{Ar\text{-}Ar}}/k_B$ $=119.8$ K (from now on this will be referred to as ε), $\varepsilon_{\mathrm{Kr\text{-}Kr}}/k_B=167.0$ K, $\varepsilon_{\mathrm{Ar\text{-}Kr}}/k_B=141.4$ K, the atomic mass for argon is $m_{\mathrm{Ar}}=39.95$ a.u. (from now on this will be referred to as m), the atomic mass for krypton is $m_{\mathrm{Kr}}=83.8$ a.u., and the cutoff radius is $r_c=2.5\sigma$.

Periodic boundary conditions are considered in the x and y directions. The smooth channel consists of 432 wall atoms and 1440 fluid atoms, while each rough wall channel consists of 504 wall atoms and 1368 fluid atoms. Wall atoms are bound on fcc sites and remain in their original positions due to the effect of an elastic spring force $\mathbf{F}=-K[\mathbf{r}(t)-\mathbf{r}_{\mathrm{eq}}]$, where $\mathbf{r}(t)$ is the vector position of a wall atom at time t, $\mathbf{r}_{\mathrm{eq}}$ is its initial lattice position vector, and K $=57.15(\varepsilon_{\mathrm{Kr\text{-}Kr}}/\sigma_{\mathrm{Kr\text{-}Kr}}^2)$ is the wall spring constant. The temperature is kept constant at $T^*=1$ (ε/k_B, k_B is Boltzmann's constant) with the application of Nosé-Hoover thermostats. An external driving force $F_{\mathrm{ext}}=0.013\,44(\varepsilon/\sigma)$ is applied along the x direction to drive the flow.

The simulation step for the system is $\Delta t=0.005\tau$ (τ is in units of $\sqrt{m\sigma^2/\varepsilon}$). In the beginning, fluid atoms are given appropriate initial velocities in order to reach the desired temperature ($T^*=1$). The system reaches the equilibrium state after a run of 2×10^6 time steps. Then, a number of nonequilibrium molecular dynamics NEMD simulations are performed, each with duration of 5×10^5 time steps.

B. Computational details

The potential energy, number density, and streaming velocity profiles are evaluated as local values at various xz
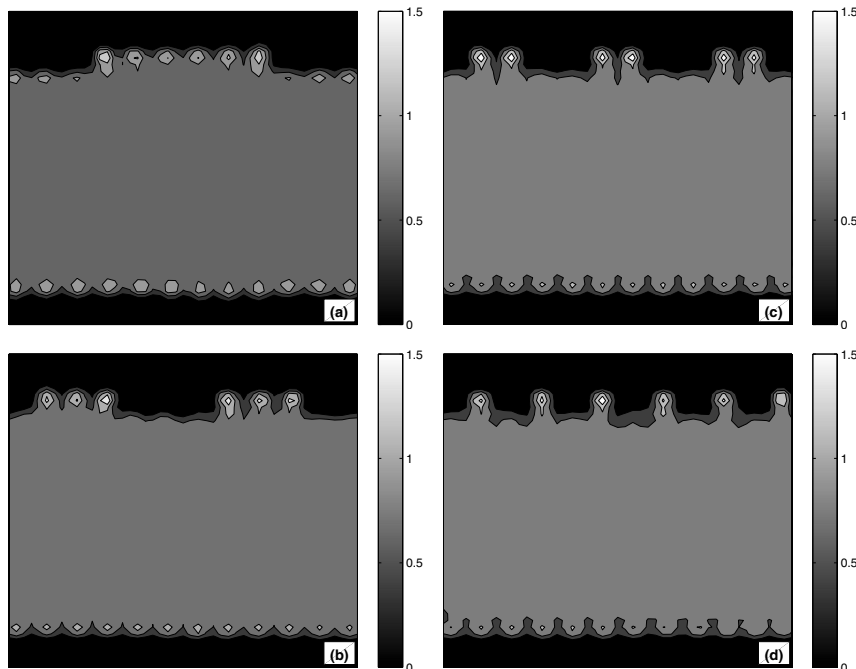
FIG. 4. Two-dimensional number density plots for $p=$ (a) 1, (b) 2, (c) 3, and (d) 6. Lighter colors denote increased fluid atom localization and black regions are the solid walls.
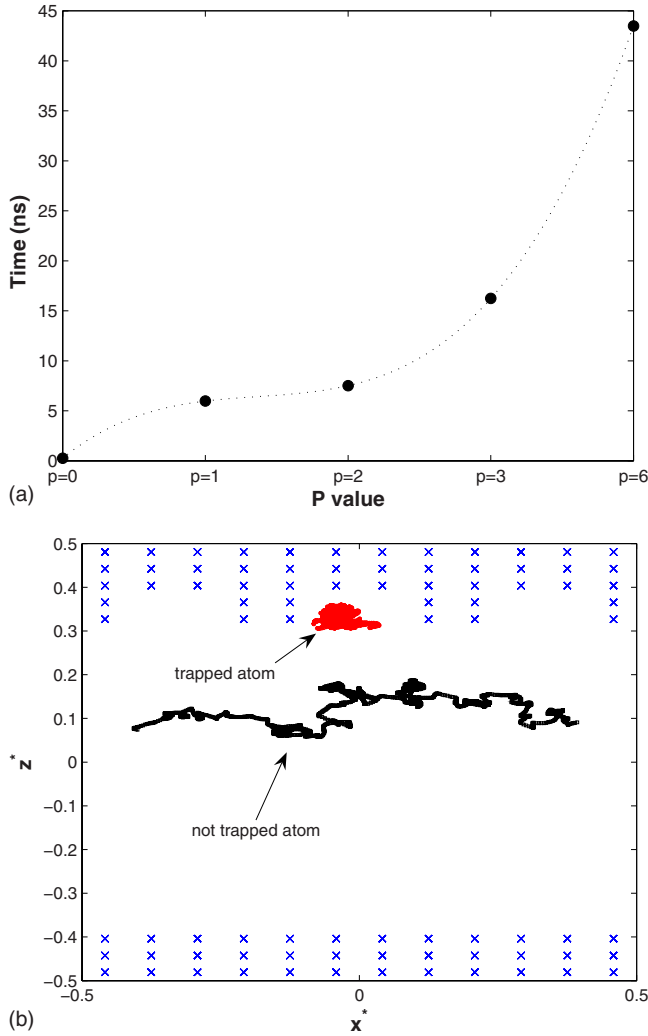
FIG. 5. (Color online) (a) Estimation of average trapping time inside cavities of a rough wall as a function of p values and (b) an example of a trapped and a nontrapped fluid atom trajectory in the xz plane (x^* and z^* are in reduced units). The points $\times$ denote the solid walls.

positions of the channels. To achieve this, the channel is divided into $m \times n$ bins in the xz plane, each one of volume $V_{\mathrm{bin}} = (L_x/m) \times L_y \times (h/n)$, where $m=48$, $n=48$. The rectangular wall consists of protrusions, cavities, and "discontinuity" regions. As shown in Fig. 1, for a discontinuity formed from a protrusion to a cavity we use the term "out-to-in" region and from a cavity to a protrusion we use the term "in-to-out" region. For example, for $p=1$ (see Fig. 1) there is one cavity, one protrusion, and two in-to-out and two out-to-in regions. The potential energy, number density, and streaming velocity are estimated in each one of these regions as local quantities.

The potential energy as a local quantity, u_{bin}, is calculated in each bin as

$$u_{\mathrm{bin}}(r_{ij}^{\mathrm{bin}}) = 4\varepsilon[(\sigma/r_{ij}^{\mathrm{bin}})^{12} - (\sigma/r_{ij}^{\mathrm{bin}})^6], \quad (2)$$

where r_{ij}^{bin} is the distance between the ith atom (located in the bin) and the jth atom. Note that the jth atom is located inside
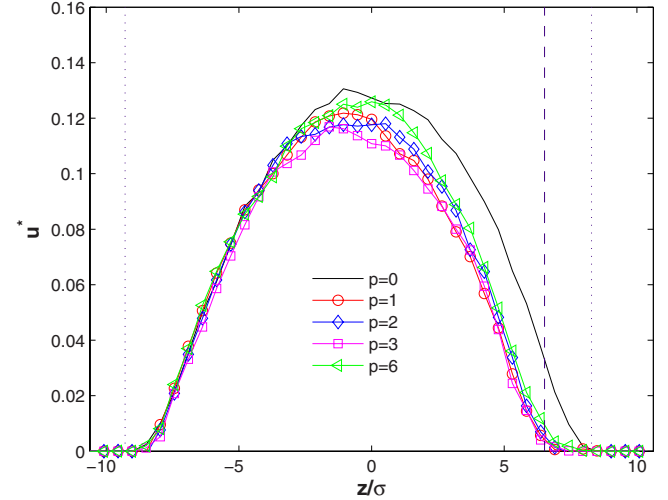
FIG. 6. (Color online) Total average streaming velocity profiles plotted over the whole channel region. Solid lines are a guide to the eye. Dashed lines denote the protrusion limits and dotted lines the cavities and lower wall limits.

the region of the ith atom interaction, but it may be outside the bin.

The slip length at the solid boundary, L_s, is calculated from the linear Navier boundary condition [25] as $L_s = u_w/(du_{w,z}/dz)|_w$, where u_w is the fluid velocity at the wall, as in [15,16,26].

III. RESULTS AND DISCUSSION

A. Potential energy distributions

Contour plots of the potential energy obtained as values averaged in time inside the nanochannels are presented in Figs. 2(a)–2(d). In all cases, the potential energy distribution does not change adjacent to the smooth wall (within statistical errors). The potential contour shape follows the wall atom placement in the fcc lattice and is not influenced by the morphology of the opposite wall. Moreover, the potential energy is uniform in the interior of the nanochannels, but presents different behavior near the rough walls.

When $p=1$ [Fig. 2(a)], on the upper rough wall, the potential energy contours follow the wall atom placement in protrusions and cavities and do not seem to affect fluid atom localization significantly in these regions. However, in the two in-to-out regions, the potential energy attains small values, and this fact is an indication that it is more probable for fluid atoms to be localized there, as the potential there is minimal. For $p=2$ [Fig. 2(b)], we observe that inside every cavity there exist two regions of high potential energy (the lighter regions) flanked by three regions of low potential energy (the darker regions). As fluid atoms tend to be localized in low potential energy regions, it is possible that fluid atoms could be trapped inside the cavities. For $p=3$ [Fig. 2(c)] we observe that inside every cavity there exists a region of high potential energy flanked by two regions of low potential energy. For $p=6$ there is only one region of low potential energy inside a cavity and it is possible for fluid atoms to be trapped there.
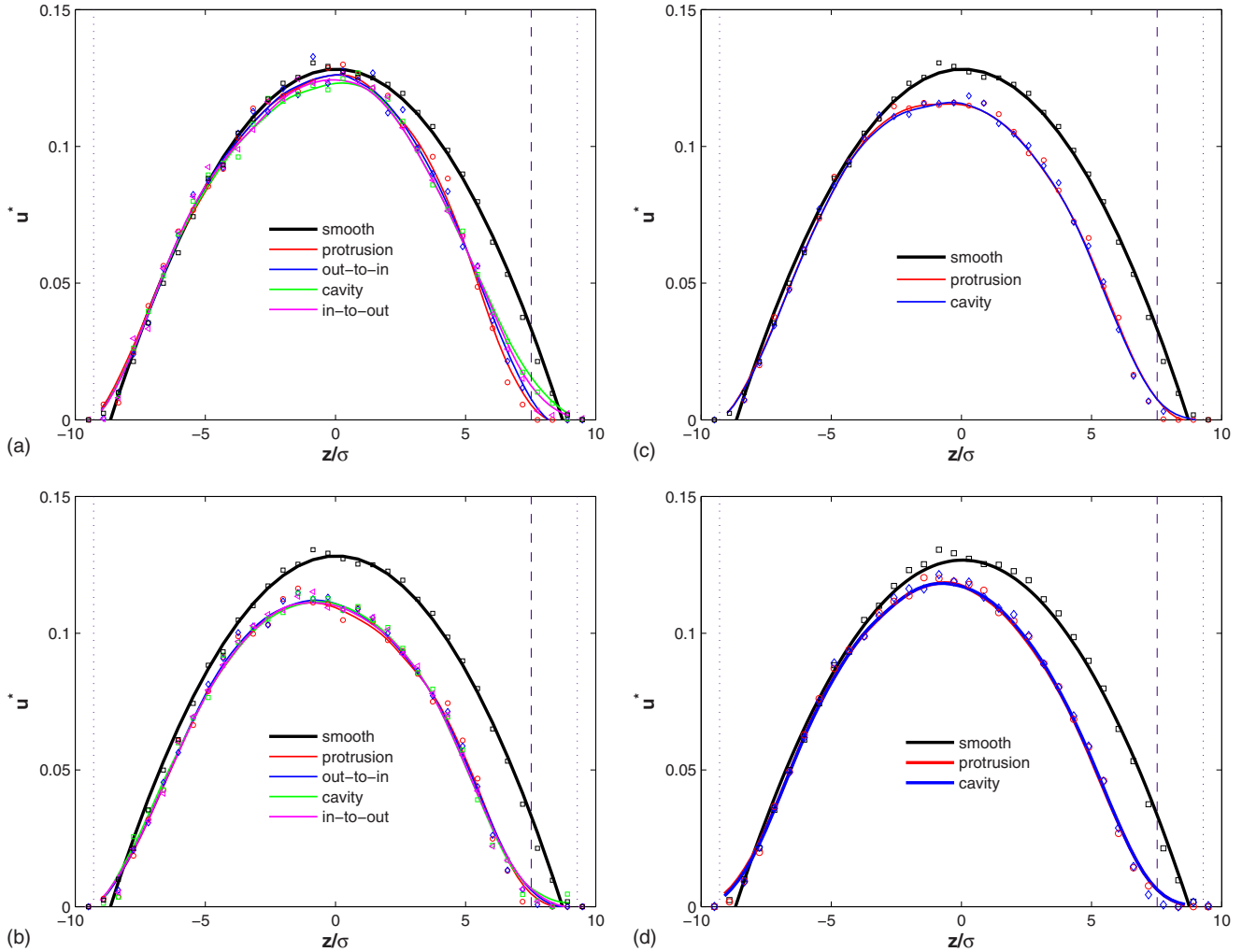
FIG. 7. (Color online) Local streaming velocity profiles at the midpoint of the protrusion, the midpoint of the cavity, and the points of discontinuity for $p=$(a) 1, (b) 2, (c) 3, and (d) 6. Solid lines are fits applied to calculated data. Dotted lines denote the cavity wall limits and dashed lines the protrusion wall limits.

The potential energy map for all channels studied reveals that the existence of rectangular anomalies at a channel wall results in the formation of low and high potential energy regions inside the rectangular grooves. This fact is expected to affect the localization of fluid atoms near a rough wall and is a possible indication of trapping of fluid atoms inside a cavity.

B. Fluid atom localization

The effect of wall roughness on fluid number density profiles as a total average value for all channel cases is presented in Fig. 3. In general, at the lower smooth wall, all channels present the same fluid atom localization with a peak in the profile occurring at a distance of about 1.5σ from the lower wall limit. At the upper rough wall, we observe a peak in the profile at 1.5σ from the rectangular cavity limit and another peak at 1.5σ from the rectangular protrusion limit. Both these two peaks are of smaller amplitude compared to the peak resulting from a smooth channel. As for the interior of the channel, it presents homogeneity in the range -5σ $<h<5\sigma$ for the smooth channel, while for all rough channels the homogeneity region extends over a smaller region $(-5\sigma<h<3.5\sigma)$. The rough wall also induced additional oscillations in the density profile in a layer of thickness 1.5σ compared to a smooth channel. The density distribution, in general, follows the shape of the rectangular walls.

In order to establish the correspondence between the potential energy maps showed in Figs. 2(a)–2(d) with fluid atom localization, we present two-dimensional number density plots in Figs. 4(a)–4(d). For $p=1$ in Fig. 4(a), we observe that the number density is significantly increased in the two in-to-out regions (more atoms localized in these regions), and this is consistent with results taken from the potential energy map [Fig. 2(a)]. For $p=2$ [Fig. 4(b)], we observe increased number density values inside the rough wall cavities. It seems that fluid atoms are trapped between the cavities since there are three subregions inside the cavities where fluid atoms are localized, as was also indicated by the potential energy map [Fig. 2(b)]. For $p=3$ and 6 [Figs. 4(c) and 4(d)] we obtain number density contours similar to those for $p=1$ and 2 at the protrusions. However, as the protrusion

length decreases, fluid atom localization inside the cavities increases.

In order to provide further evidence of fluid atom trapping inside rough wall cavities, we estimate the average time that fluid atoms remain inside cavity boundaries for every channel studied. At the beginning of the simulation, we detect and count all fluid atoms that are localized inside all cavity boundaries. All trapped fluid atom trajectories are saved till the end of the simulation and the average time for which fluid atoms remain inside a cavity is extracted. Results are depicted in Fig. 5(a), where we observe that, as the length of the protrusions decreases (p increases), fluid atoms previously located inside a cavity tend to remain trapped there for a longer time. Characteristic trajectories of a trapped and a free-running fluid atom in the xz level for $p=3$ are shown in Fig. 5(b). The trapped atom circulates inside the cavity for a considerable time interval and does not escape during this period into the interior of the channel.

In conclusion, from the detailed investigation of two-dimensional density profiles presented here, in connection with the potential energy map [Figs. 2(a)–2(d)], most importantly, from the timing analysis of fluid atom trajectories, there is conclusive evidence that fluid atoms are trapped inside wall cavities and this effect becomes more pronounced as the groove characteristic length decreases.

C. Streaming velocity profiles and slip length

Figure 6 shows streaming velocity profiles averaged in time and space [i.e., $\overline{v_x}(z)$] in all rough channels considered. We observe that, although maximum velocity values are not significantly affected by the presence of roughness (at least for the cases studied here where the roughness amplitude is about 10% of the channel width), the shape of the velocity profile is significantly affected in the upper half of the channel (i.e., $-2\sigma \leq h \leq 8.5\sigma$) by the presence of the rough wall.

In Fig. 7, we present local streaming velocity profiles of the rough wall for $p=1$, 2, 3, and 6, and we compare them to the velocity profile of a smooth channel. For $p=1$ [Fig. 7(a)] all velocity profiles near the rough wall are suppressed to the left and cannot be parabolically fitted (fits shown here are smoothing splines). We observe that for $-9\sigma \leq h \leq 0$ (the lower half of the channel) velocity profiles for $p=0$ (the smooth channel) and all regions of $p=1$ are quite similar. The rough wall has induced suppression in the velocity profiles at protrusions and out-to-in regions for $0 \leq h \leq 9\sigma$, as expected, since wall protrusions enter the fluid area and the available channel width is decreased. However, we also observe suppression to the left on velocity profiles at the cavities and the in-to-out regions for $0 \leq h \leq 9\sigma$, where the available channel width is similar to that of a smooth channel. This means that fluid atoms inside a cavity for $p=1$ have clearly smaller velocity values compared to a smooth channel. Having in mind that fluid atoms are localized inside the cavities (as shown in the previous section) we come to the conclusion that fluid atoms tend to be immobilized inside the wall cavities.

For $p=2$ [Fig. 7(b)] we observe that all local velocity profiles in protrusions, cavities, and the transitional regions
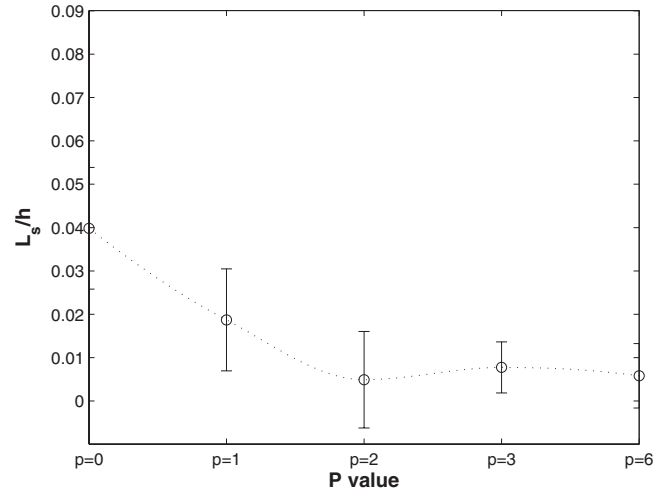
FIG. 8. Slip length at the rough wall as a function of p.

have similar shape and smaller maximum values compared to a smooth channel. We also obtain smaller velocity values inside the cavities compared to a smooth channel and even smaller than for $p=1$ [Fig. 7(a)]. It seems that, as the cavities become narrower from $p=1$ to $p=2$, the velocity at the rough wall decreases. This is the trend that we also observe for $p=3$ and 6 [Figs. 7(c) and 7(d), respectively], where we obtain velocity values close to zero near the rough wall. We also note that we do not have a monotonic behavior for the maximum velocity values as p increases from $p=0$ to 6, but we can conclude that all maximum velocity values are smaller in the rough channel cases compared to a smooth one.

Estimates of the slip length on the rough wall as a function of p are plotted in Fig. 8. We observe that slip length presents a clear decaying behavior from $p=0$ to 2 and approaches zero for $p=3$ and 6. We attribute this behavior to the fact that fluid atom velocity values near a rough wall decrease, as shown in Figs. 7(a)–7(d), as a result, slip on the rough boundary diminishes.

This is consistent with slip length behavior observed in sinusoidally rough nanochannels [17]. In [27], a comparison of slip length as a function of the "slope parameter $k\alpha$" of the rough wall between MD simulations and analytical predictions from [28] is made. Our results are consistent with the numerical values reported in [27]. No comparison can be made with the analytical solution because our system's parameters are beyond the range of applicability of the asymptotic theory.

IV. CONCLUSIONS

We have presented nonequilibrium molecular dynamics simulations of nanoflow of liquid argon between krypton walls with five different lengths of periodic rectangular roughness. The effect of wall roughness on potential energy distribution, fluid atom localization, streaming velocity profiles, and slip length at the boundary is significant and should be taken into account in most nanofluidic systems, since it seems rare for a surface to be characterized as smooth at the nanoscale.

The potential energy map for all rough channels studied shows that there exist low and high potential energy regions inside the rectangular cavities that have different behavior as the length of the groove decreases (as p increases). This fact affects fluid atom localization near a rough wall and is an indication of trapping of fluid atoms inside a cavity.

Two-dimensional density plots reveal inhomogeneity near the solid boundary, especially near the rough walls. We presented number density contour plots that show that fluid atoms tend to be localized inside rough wall cavities. As the cavities become narrower, this localization increases.

As far as velocity profiles are concerned, we showed that the maximum value of streaming velocity in the center of the channel is not significantly affected by the presence of roughness. In general, velocity profiles are suppressed in the upper half of the channel where the rough wall is present, while they are similar to those of a smooth channel in the lower half of the channel. From the velocity profiles presented in this paper, we showed that as the rectangular wall cavities become narrower (as the p value increases) velocity values inside the cavities decrease and fluid atoms tend to be trapped inside them. As a result, slip on the boundary diminishes as fluid atoms are trapped inside the cavities.

The existence of wall roughness is a significant feature that has to be borne in mind when it comes to designing flow systems at the nanoscale. One has to take seriously into consideration the effect of fluid atoms that are being trapped inside the wall anomalies. Depending on the application, different combinations of materials and wall shapes could be used to influence flow properties.

[1] J. Koplik, J. R. Banavar, and J. F. Willemsen, Phys. Fluids A **1**, 781 (1989).

[2] S. A. Somers and H. T. Davis, J. Chem. Phys. **96**, 5389 (1992).

[3] G. E. Karniadakis, A. Beskok, and N. Aluru, *Microflows and Nanoflows: Fundamentals and Simulation* (Springer, New York, 2002).

[4] K. P. Travis, B. D. Todd, and D. J. Evans, Phys. Rev. E **55**, 4288 (1997).

[5] K. P. Travis and K. E. Gubbins, J. Chem. Phys. **112**, 1984 (2000).

[6] J. S. Hansen and J. T. Ottesen, Microfluid. Nanofluid. **2**, 301 (2006).

[7] E. Akhmatskaya, B. D. Todd, P. J. Daivis, D. J. Evans, K. E. Gubbins, and L. A. Pozhar, J. Chem. Phys. **106**, 4684 (1997).

[8] A. S. Ziarani and A. A. Mohammad, Microfluid. Nanofluid. **2**, 12 (2005).

[9] U. Heinbuch and J. Fischer, Phys. Rev. A **40**, 1144 (1989).

[10] N. V. Priezjev, A. A. Darhuber, and S. M. Troian, Phys. Rev. E **71**, 041608 (2005).

[11] G. Nagayama and P. Cheng, Int. J. Heat Mass Transfer **47**, 501 (2004).

[12] G. Mo and F. Rosenberger, Phys. Rev. A **42**, 4688 (1990).

[13] N. V. Priezjev, J. Chem. Phys. **127**, 144708 (2007).

[14] T. M. Galea and P. Attard, Langmuir **20**, 3477 (2004).

[15] B. Y. Cao, M. Chen, and Z. Y. Guo, Phys. Rev. E **74**, 066311 (2006).

[16] A. S. Ziarani and A. A. Mohammad, in *Proceedings of the 17th IASTED International Conference, Modelling and Simulation, Montreal, Canada, 2006*, edited by R. Wamkeue (ACTA Press, Anaheim, CA, 2006) pp. 585–590.

[17] A. Jabbarzadeh, J. D. Atkinson, and R. I. Tarner, Phys. Rev. E **61**, 690 (2000).

[18] D. Kim and E. Darve, Phys. Rev. E **73**, 051203 (2006).

[19] M. Sbragaglia, R. Benzi, L. Biferale, S. Succi, and F. Toschi, Phys. Rev. Lett. **97**, 204503 (2006).

[20] J. Harting, C. Kunert, and H. J. Herrmann, Europhys. Lett. **75**, 328 (2006).

[21] J. Philip, Z. Angew. Math. Phys. **23**, 960 (1972).

[22] E. Lauga and H. Stone, J. Fluid Mech. **489**, 55 (2003).

[23] J. Ou, B. Perrot, and J. P. Rothstein, Phys. Fluids **16**, 4635 (2004).

[24] J. Ou and J. P. Rothstein, Phys. Fluids **17**, 103606 (2005).

[25] S. Goldstein, *Modern Developments in Fluid Dynamics: An Account of Theory and Experiment Relating to Boundary Layers, Turbulent Motion and Wakes* (Dover, New York, 1965), Vol. 2.

[26] B. Y. Cao, M. Chen, and Z. Y. Guo, Int. J. Eng. Sci. **44**, 927 (2006).

[27] N. V. Priezjev and S. Troian, J. Fluid Mech. **554**, 25 (2006).

[28] D. Einzel, P. Panzer, and M. Liu, Phys. Rev. Lett. **64**, 2269 (1990).